Force-Free Electromagnetic Pulses in a Laboratory Plasma

R. L. Stenzel and J. M. Urrutia
Department of Physics, University of California, Los Angeles, California 90024-1547
(Received 19 March 1990)

A short, intense current pulse ($I=150$ A, $\Delta t\simeq 0.2$ μs, $N\simeq 2\times 10^{14}$ electrons) is drawn from an electrode immersed in a magnetized afterglow plasma ($n\simeq 2\times 10^{11}$ cm^{-3}, $kT_e\simeq 1.3$ eV, $B_0=10$ G). The induced magnetic field $\mathbf{B}(\mathbf{r},t)$ assumes the shape of a helical double vortex which propagates along $\mathbf{B}_0$ through the uniform plasma as a whistler mode. The observations support a prediction of force-free ($\mathbf{J}\times\mathbf{B}+ne\mathbf{E}=0$) electromagnetic fields and solitary waves. Energy and helicity are approximately conserved.

PACS numbers: 52.35.Hr, 52.35.Mw, 52.40.Db, 52.70.Ds

Force-free magnetic-field configurations are of fundamental interest in plasma physics[1,2] and of particular relevance to space plasmas[3] and magnetic confinement of fusion plasmas.[4] In such configurations, the magnetic force $\mathbf{J}\times\mathbf{B}$ vanishes, implying that the current $\mathbf{J}$ flows exactly along the magnetic field $\mathbf{B}$. While the existence of such ideal configurations has been questioned,[2] the balance between magnetic and pressure forces, $\mathbf{J}\times\mathbf{B}=\nabla p$, is a well-established concept of MHD equilibrium.[5] However, the MHD description of plasmas is a special case ($\omega<\omega_{ci}$, $p/\nabla p\gg r_{ci}$), and it is also of interest to consider the case of rapidly varying fields ($\omega\gg\omega_{ci}$). For such electromagnetic fields, both magnetic *and* electric forces have to be considered in the force balance. Thus, the condition for force-free electromagnetic fields in a uniform plasma is given by[6] $\mathbf{J}\times\mathbf{B}+ne\mathbf{E}=0$. Analysis of this equation predicts oscillatory solutions, i.e., a localized force-free electromagnetic solitary wave with both transverse (inductive) and longitudinal (space-charge) electric-field components.[6] In the present Letter, we report on experimental observations of such field configurations. We generate a time-varying electromagnetic field by the pulsed extraction of electrons to a positive electrode. Strong electric fields (space charge and inductive) are generated. Because of the short pulse length, the ion density remains essentially constant. The electromagnetic field evolves into a nearly force-free localized pulse that propagates along the uniform dc magnetic field B_0 as an intense ($B_{\text{wave,max}}\simeq B_0$) whistler wave packet with little change in energy and helicity. These properties distinguish our findings from traditional MHD force-free field configurations, e.g., spheromaks.[4]

The experiment is performed in the afterglow of a uniform ($n/\nabla n\simeq 1$ m), collisionless ($\nu_{ei}/\omega_{ce}\simeq 0.02$), pulsed discharge (1 m diameter, 2.5 m length) immersed in a uniform axial magnetic field $\mathbf{B}_0$ (Fig. 1). A pulsed current (150 A, 0.2-μs half-width) is established between a 4-cm-diam-plane, positively biased electrode and the chamber wall. The time-varying magnetic field $\mathbf{B}(\mathbf{r},t)$ is mapped with three orthogonal magnetic loops (1 cm diameter, mounted at the end of a single shaft) in space and time (B_x,B_y,B_z vs x,y,z,t) from repeated, highly reproducible ($\delta n/n\lesssim 1\%$, $t_{\text{jitter}}\lesssim 10$ ns) experiments. From the complete knowledge of $\mathbf{B}_{\text{tot}}=\mathbf{B}_0+\mathbf{B}(\mathbf{r},t)$, we calculate the total (conduction plus displacement) current density $\mathbf{J}=\nabla\times\mathbf{B}/\mu_0$, the vector potential $\mathbf{A}=(\mu_0/4\pi)\int(\mathbf{J}/R)dV$, the magnetic helicity $K=\int\mathbf{A}\cdot\mathbf{B}\,dV$, the inductive electric field $\mathbf{E}_i=-\partial\mathbf{A}/\partial t$, and the force field $\mathbf{J}\times\mathbf{B}_{\text{tot}}$.

The time-varying component of the magnetic energy density $B^2(\mathbf{r},t)/2\mu_0$ propagates as shown in Fig. 2. The electrode at $z\simeq -5$ cm draws current at $0<t\lesssim 0.5$ μs (0.2-μs half-width). The perturbation propagates along B_0 at a speed $v_z\simeq 6.5\times 10^7$ cm/s which is comparable to the group velocity of a whistler wave packet,[7]

$$v_g=2c(1-\omega/\omega_c)^{3/2}(\omega\omega_c/\omega_p^2)^{1/2}\simeq 6\times 10^7\ \text{cm/s}$$

at $B_0=10$ G, $n_e\simeq 2\times 10^{11}$ cm^{-3}, and $\omega/2\pi\simeq\Delta t_{\text{packet}}^{-1}\simeq v_z/\Delta z_{\text{packet}}\simeq 2$ MHz. Although this value happens to be close to the electron thermal speed, earlier dispersion measurements[8] have established that whistlers rather than particles create the field perturbation. The peak magnetic energy density of the wave exceeds the particle energy density by almost an order of magnitude [$B^2(\mathbf{r},t)/2\mu_0\simeq 7nkT_e$], but decreases during propagation. Dispersive wave spread rather than damping accounts for the energy-density decay since the volume integral of the perturbation energy is nearly conserved, as discussed below.

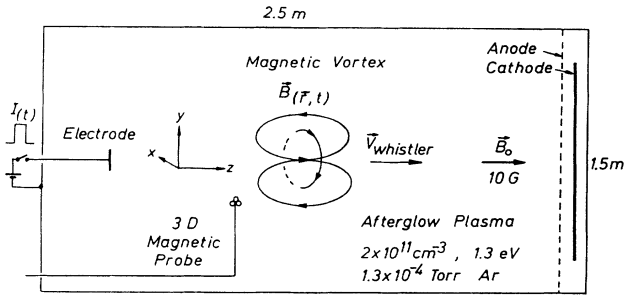

FIG. 1. Schematic view of the plasma device used for exciting and diagnosing force-free propagating electromagnetic pulses (illustrated in a highly idealized manner).

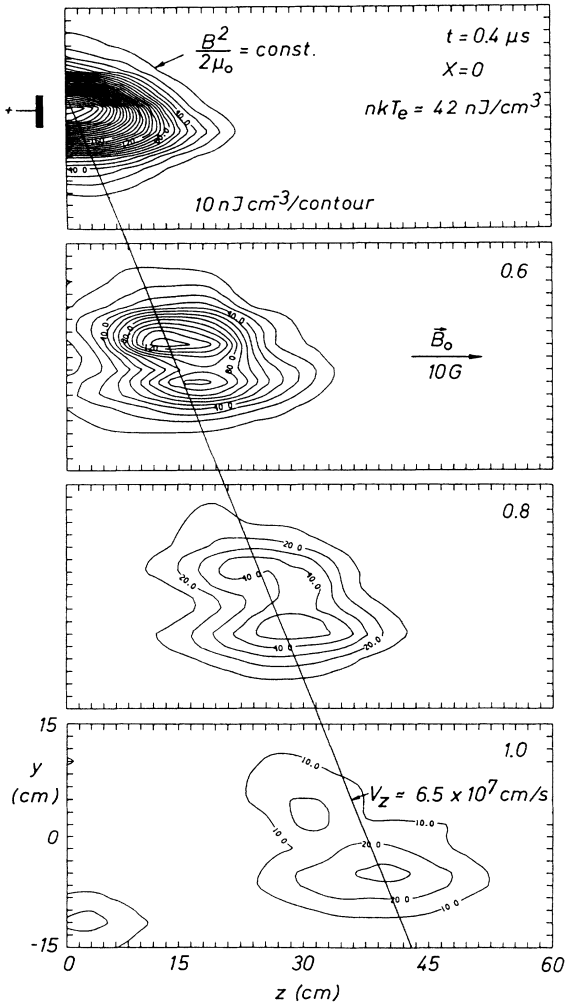

FIG. 2. Contours of constant perturbed magnetic energy density $B^2(0,y,z,t)/2\mu_0$ at different times t after drawing a 150-A, 0.5-μs current pulse from a plane electrode (B_0 not included). The perturbation propagates as a whistler wave packet along $\mathbf{B}_0$.

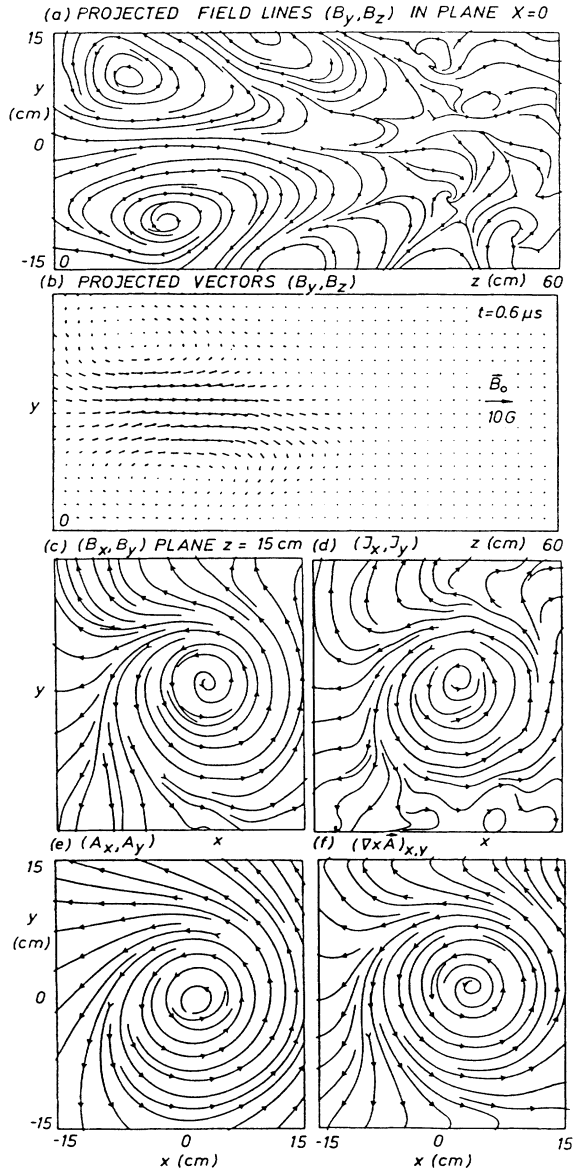

FIG. 3. Spatial characteristics of the propagating fields at a fixed time $t=0.6$ μs. (a) Magnetic-field lines and (b) magnetic vectors $\mathbf{B}(\mathbf{r},t)$ projected into the y-z plane ($x=0$) showing a cut through a localized solenoidal field. (c) Magnetic-field lines projected into the x-y plane transverse to the solenoidal field at $z=15$ cm. The spiraling poloidal field is linked with the solenoidal field. (d) Current density $\mathbf{J}=\nabla\times\mathbf{B}/\mu_0$, projected into the same x-y plane, suggesting field-aligned currents. (e) The vector potential $\mathbf{A}$, calculated from $\mathbf{J}$, projected into the x-y plane. (f) Magnetic-field lines calculated via $\mathbf{B}=\nabla\times\mathbf{A}$ showing excellent agreement with the measured magnetic field (c).

The topology of the time-dependent three-dimensional field is illustrated in Fig. 3 by various two-dimensional projections. Figures 3(a) and 3(b) display magnetic-field lines and vectors, respectively, in the central y-z plane. The major feature is a finite-length solenoidal field ($10 \lesssim z \lesssim 30$ cm) closed via two magnetic vortices. Weaker features include magnetic islands of alternating vorticity (e.g., at $y=-15$ cm, $z=30$ and 45 cm) aligned along a diverging path from the exciter. Figures 3(c)–3(f) show projections of the fields into a transverse x-y plane at $z=15$ cm. Based on the probe dimensions and data-point spacing (1.5 cm), structures of scale $\Delta l \geq 2$ cm are properly resolved. The magnetic-field lines [Fig. 3(c)] exhibit a large central vortex which is created by axial plasma currents, $J_z > 0$. Note that the vorticity reverses sign at the periphery, indicating the presence of axial return currents, $J_z < 0$. The current density $\mathbf{J}=\nabla\times\mathbf{B}/\mu_0$, projected into the transverse x-y plane [Fig. 3(d)], has the same topology as the magnetic field, suggesting that $\mathbf{J}$ and $\mathbf{B}$ are approximately parallel. Again, the current at the periphery is opposite to that at the center. The transverse current [Fig. 3(d)] gives rise to

the axial solenoidal magnetic field [Fig. 3(b)] which in turn is nearly parallel to the axial current density. Thus, both magnetic field and current density form linked vortices. The configuration can be modeled by two helical field-current systems: one near the center of the pulse and a reverse one near the periphery. Their fields cancel at large distances, consistent with the fact that the wave energy is localized in a bounded wave packet.

In order to determine magnetic helicity and induced electric fields, the vector potential has been calculated from first principles via

$$\mathbf{A}(\mathbf{r}) = (\mu_0/4\pi)\int\int\int [\mathbf{J}(\mathbf{r}')/|\mathbf{r}-\mathbf{r}'|]dV'$$

[Fig. 3(e)] using the available data which includes most of the currents of interest. Currents outside the volume mapped do not appear to be as important as those composing the central current system. This is confirmed by calculating $\nabla\times\mathbf{A}$ [Fig. 3(f)] and finding good agreement with $\mathbf{B}$ in direction [Fig. 3(c)] and magnitude (not shown) as expected from the definition $\nabla\times\mathbf{A}=\mathbf{B}$. The magnetic helicity density $\mathbf{A}\cdot\mathbf{B}$ (see Fig. 5, inset) is localized to the wave packet and propagates similarly to the magnetic energy density $\mathbf{B}\cdot\mathbf{B}/2\mu_0$. On axis, the major contribution to the helicity comes from A_zB_z; off axis it is from $A_xB_x+A_yB_y$.

The inductive electric field, $\mathbf{E}_i=-\partial\mathbf{A}/\partial t$, projected into the x-y plane ($z=15$ cm) is shown in Fig. 4(a). The $\mathbf{E}$ field exhibits a curl which changes sign as the axial flux through the x-y plane, $\int\int B_z\,dx\,dy$, varies during the pulse propagation. The axial component of the inductive electric field, $-\partial A_z/\partial t$, shown in Fig. 4(b), is associated with the time variation of (B_x,B_y). In addition to the inductive field, there must be a space-charge electric field since the collection of electrons at the electrode creates a significant local charge imbalance ($\Delta Q \gtrsim 10^{14}\times e$). Although this field contribution has not been measured directly, it can be reasonably estimated as follows: The component of the current density along the local total magnetic field, $\mathbf{J}\|\mathbf{B}_{\rm tot}$, is predominantly a conduction current ($\nu_{ei}\simeq 3\times10^6$ Hz $<\omega_{\rm packet}\simeq 1.3\times10^7$ rad/s) which is related via Ohm's law to the net electric field (space charge plus inductive) by $E_\parallel=\eta_\parallel J_\parallel$, where $\eta_\parallel=m\nu_{ei}/ne^2$ is the Spitzer resistivity ($\eta_\parallel\simeq 6\times10^{-2}$ Ω cm). The lack of significant wave-energy loss (shown in Fig. 5 and discussed below) justifies the assumption of classical resistivity. The net electric-field component across the local magnetic field $\mathbf{B}_{\rm tot}$ is found from $E_\perp\simeq\mathbf{J}\times\mathbf{B}_{\rm tot}/ne$, assuming that polarization currents are negligible in comparison to Hall currents ($\omega\ll\omega_{ce}$). Combining $\mathbf{E}_\parallel$ and $\mathbf{E}_\perp$ yields the three-dimensional vector field $\mathbf{E}=-\nabla\phi-\partial\mathbf{A}/\partial t$. Figure 4(c) shows its projection (E_x,E_y) into the x-y plane and Fig. 4(d) displays the much smaller E_z component in the same plane

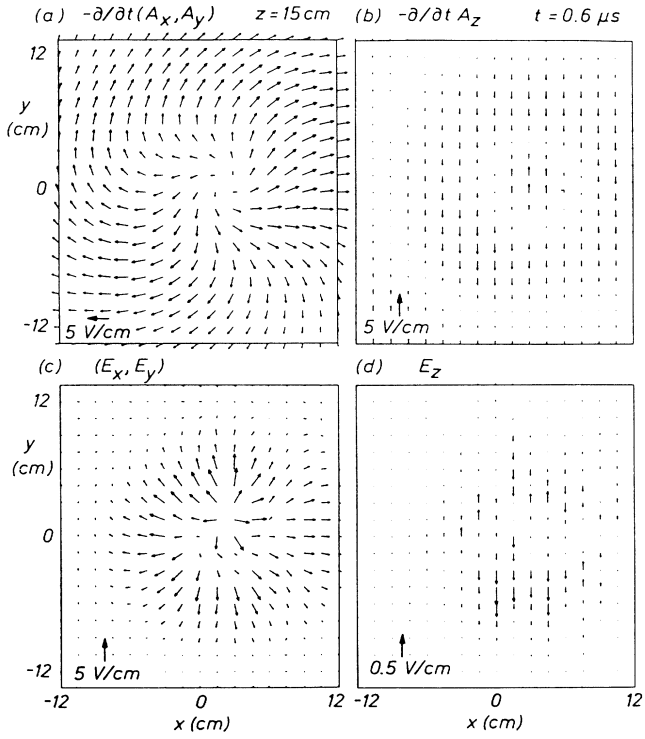

FIG. 4. Electric fields at a fixed time in the x-y plane at $z=15$ cm. (a) Projection of the inductive electric field $-\partial(A_x,A_y)/\partial t$. (b) Axial component $-\partial A_z/\partial t$ displayed along the $\pm y$ direction. (c) Total electric field, $\mathbf{E}=-\nabla\phi-\partial\mathbf{A}/\partial t$, projected into the x-y plane. (d) Axial component E_z displayed along the $\pm y$ direction (note change of scale).

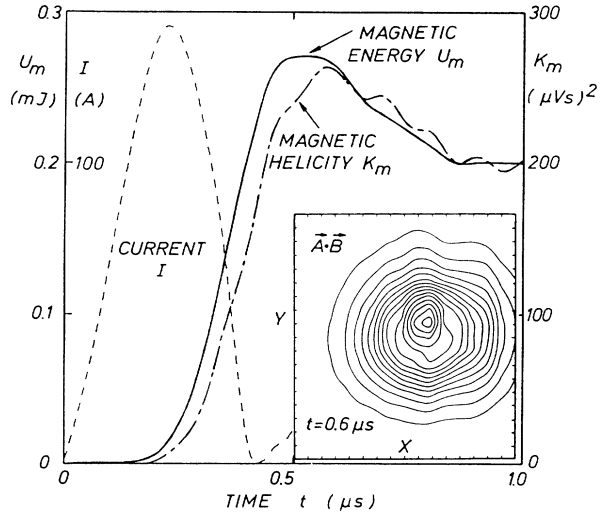

FIG. 5. Time dependence of the magnetic energy $U_m=\int[B^2(\mathbf{r},t)/2\mu_0]\,dV$ and helicity $K_m=\int\mathbf{A}(\mathbf{r},t)\cdot\mathbf{B}(\mathbf{r},t)\,dV$ within the measurement volume ($30\times30\times60$ cm^3), showing approximate conservation of U_m and K_m during the propagation of the electromagnetic pulse. The externally measured current wave form is also shown for comparison. Inset: Contour plot of magnetic helicity density $\mathbf{A}(\mathbf{r},t)\cdot\mathbf{B}(\mathbf{r},t)$ (80 G^{2}cm/contour) at $t=0.6$ μs in the same x-y plane as in Figs. 3(c)–3(f). It is localized similarly to $B^2/2\mu_0$ (Fig. 2).

($E_z > 0$ drawn in the $+y$ direction, $E_z < 0$ in the $-y$ direction). The irrotational electric field, $-\nabla\phi$, may be found by subtracting the rotational contribution, $-\partial\mathbf{A}/\partial t$, from the total field. Since it is observed that $|E_\parallel| \ll |\partial\mathbf{A}_\parallel/\partial t|$ [note the order-of-magnitude scale change in Figs. 4(b) and 4(d)], the large inductive electric field along $\mathbf{B}_{\rm tot}$ must be canceled by a comparable space-charge electric field. The center of the magnetic pulse must therefore assume a large positive potential ($\int\nabla\phi\cdot d\mathbf{l} \simeq +100$ V) which is comoving with the wave. The perpendicular field $\mathbf{E}_\perp$ has rotational and irrotational contributions of comparable magnitudes which, in general, need not cancel, on account of the low cross-field conductivity $\sigma_\perp \ll \sigma_\parallel$.

The magnetic force density $\mathbf{J}\times\mathbf{B}_{\rm tot}$ has also been calculated. While the current density $\mathbf{J}$ is directed predominantly along the local total magnetic field, $|\mathbf{J}\cdot\mathbf{B}_{\rm tot}| > |\mathbf{J}\times\mathbf{B}_{\rm tot}|$, there is a pronounced, radially outward pointing force density in the x-y plane [similar to Fig. 4(c)]. This magnetic force is balanced by electric forces ($\mathbf{J}\times\mathbf{B}_{\rm tot} + ne\mathbf{E} \simeq 0$). The axial force density is negligibly small, $|\mathbf{J}\times\mathbf{B}_{\rm tot}|_z \ll |\mathbf{J}\times\mathbf{B}_{\rm tot}|_{x,y}$, and thus the electromagnetic field is nearly force free. This conclusion is supported by two other observations: (1) The pulsed current has been varied by orders of magnitude (50 mA–150 A) without observing fundamental differences in magnetic-field topologies or propagation characteristics. (2) The intense nonuniform field [$B^2(\mathbf{r},t)/2\mu_0 \gg nkT_e$] propagates at a constant speed ($\mathbf{a} = d\mathbf{v}/dt \simeq 0$) with small geometric spread determined by whistler wave dispersion[7] rather than field amplitude.

Finally, the conservation and dissipation of global quantities (energy, helicity) has been investigated. Figure 5 shows the volume-integrated energy density $\int[B^2(\mathbf{r},t)/2\mu_0]dV$ and helicity density $\int\mathbf{A}(\mathbf{r},t)\cdot\mathbf{B}(\mathbf{r},t)\,dV$ versus time. For comparison, the time development of the externally measured current is also displayed. In contrast to the local densities, which decrease due to wave spread within the ray cone,[7] the total energy and helicity decay slowly, mostly due to wave propagation out of the finite measurement volume. The small time delay between helicity and energy is of yet unknown origin.

In conclusion, the observations presented in this Letter show the existence of an essentially force-free, intense, localized electromagnetic field, supported by a collisionless plasma, consistent with theoretical predictions.[6] Such highly nonlinear structures are of fundamental interest (electromagnetic solitons), and of possible relevance to fusion (rf heating) and space plasmas (electromagnetic impulse).

The authors acknowledge stimulating discussions with Dr. V. Osherovich and N. A. Salingaros. This research was supported by NSF Grants No. PHY 87-13829 and No. ATM 87-02793, and by NASA NAGW-1570.

[1]S. Lundquist, Ark. Fys. **2**, 381 (1950); L. Woltjer, Proc. Natl. Acad. Sci. U.S.A. **44**, 489 (1958); J. B. Taylor, Phys. Rev. Lett. **33**, 1139 (1974).

[2]N. A. Salingaros, J. Phys. A **19**, 705 (1986); Mod. Phys. Lett. B **3**, 1285 (1989).

[3]R. Lüst and A. Schlüter, Z. Astrophys. **34**, 263 (1954); J. Heyvaerts and E. R. Priest, Astron. Astrophys. **137**, 63 (1984).

[4]H. A. B. Bodin and A. A. Newton, Nucl. Fus. **20**, 1255 (1980); A. Janos, Phys. Fluids **29**, 3342 (1986); K. Kawai, Z. A. Pietrzyk, and H. T. Hunter, Phys. Fluids **30**, 2561 (1987).

[5]F. F. Chen, *Introduction to Plasma Physics* (Plenum, New York, 1974), Chap. 6.

[6]V. A. Osherovich and E. B. Gliner, Sol. Phys. **117**, 391 (1988).

[7]R. A. Helliwell, *Whistlers and Related Ionospheric Phenomena* (Stanford Univ. Press, Stanford, 1965), Chap. 3.

[8]R. L. Stenzel and J. M. Urrutia, J. Geophys. Res. **95**, 6209 (1990).